

# Monitoring of phreatic eruptions using Interferometry on Retrieved Cross-Correlation Function from Ambient Seismic Noise: Results from Mt. Ruapehu, New Zealand

A. Mordret <sup>a,b</sup>, A.D. Jolly <sup>a,\*</sup>, Z. Duputel <sup>b</sup>, N. Fournier <sup>a</sup>

<sup>a</sup> GNS Science, Wairakei Research Centre, Private Bag 2000, Taupo, New Zealand

<sup>b</sup> Institut de Physique du Globe de Strasbourg (UMR 7516 CNRS, Université de Strasbourg/EOST), 5 rue René Descartes, 67084 Strasbourg cedex, France

## ARTICLE INFO

### Article history:

Received 29 April 2009

Accepted 8 January 2010

Available online 28 January 2010

### Keywords:

ambient seismic noise  
Coda Wave Interferometry  
Mt. Ruapehu  
volcano monitoring  
seismic velocity variations

## ABSTRACT

Since the last major eruption in 1995–96 Mt. Ruapehu has erupted twice, on 4 October 2006 and on 25 September 2007. These events occurred without any clear precursors and were mostly phreatic explosions. The technique of “Interferometry on Retrieved Cross-Correlation Function from Ambient Seismic Noise” (IRCCASN) is used to monitor subtle temporal changes of Mt. Ruapehu's elastic properties. The computation of Cross-Correlation Functions of seismic noise recorded at several stations around the volcano allowed us to observe variations during the 2006 eruption period. The comparison between a Reference Cross-Correlation Function and a Current Cross-Correlation Function allows us to infer relative seismic velocity variations. A 0.8% decrease of relative seismic velocity in the edifice, starting two days before the 2006 eruption, was observed. This drop is due to a reversible and ephemeral effect, which can be attributed to a pressurization of a magma pocket beneath the east flank of Ruapehu due to new magma entering a small reservoir. This pressure increase produced an inflation of the east flank of Ruapehu and opened fractures in this area leading to a localised drop of seismic velocity. We conducted the same analysis for the 2007 eruption but no significant seismic velocity variation was observed. This difference is possibly due to the varying time scales of pressurization for the two events and also the IRCCASN time resolution. An analysis of the seismicity before these two eruptions allows us to propose a conceptual model which explains the velocity drop for the 2006 eruption and the lack of velocity variations for the 2007 eruption. Since there was no surface deformation recorded by the GeoNet GPS network, we modelled the maximum radius and pressure change for a simple Mogi point source at 5 km depth that produced no deformation. We inferred the maximum fresh magma volume of  $\sim 0.0017 \text{ km}^3$  entering the reservoir as a detectability threshold for GPS ground deformation measurements.

© 2010 Elsevier B.V. All rights reserved.

## 1. Introduction

Mt. Ruapehu is a 250,000 year-old andesitic volcano located at the southern end of the Taupo Volcanic Zone (TVZ), New Zealand (Bryan and Sherburn, 2003; Hackett and Houghton, 1989), a back-arc region characterised by extension, intense volcanism and a high heat flux (Bibby et al., 1995). Of the 8 major historic eruptions since 1945, those occurring in 1969, 1975, 1988, 2006 and 2007 (Sherburn et al., 1999) had no clear precursors and occurred without warning. These events are mostly phreatic and the explosion deposits are confined to the summit area. However, they remain hazardous due to the proximity of recreational hikers, climbers and skiers. These eruptions can also displace Crater Lake water into the Whangaehu and other catchments,

producing lahars which may flow down the ski fields and cross hiking tracks around Ruapehu (Manville et al., in preparation). They also produce ballistics which may injure climbers near the Crater Lake (Kilgour et al., 2009). This paper highlights the need to better understand and attempt to provide warning for this common eruption type at Ruapehu and presents results of the “Interferometry on Retrieved Cross-Correlation Functions from Ambient Seismic Noise” (IRCCASN) technique for the 4 October 2006 and 25 September 2007 eruptions.

## 2. The 2006–2007 eruptive period setting

The last major eruptive episode at Ruapehu occurred in 1995–96, resulting in the emptying of the Crater Lake (Bryan and Sherburn, 1999) and creating an 8 m-thick dam of tephra and volcanoclastic material on the former outlet of the lake. During the ten following years the Crater Lake refilled gradually, about equally due to climatic contributions and to condensed steam from the subaqueous hydrothermal

\* Corresponding author. Tel.: +64 7 376 0133; fax: +64 7 374 8199.

E-mail addresses: [aurelien.mordret@gmail.com](mailto:aurelien.mordret@gmail.com) (A. Mordret), [A.Jolly@gns.cri.nz](mailto:A.Jolly@gns.cri.nz) (A.D. Jolly), [zacharie.duputel@eost.u-strasbg.fr](mailto:zacharie.duputel@eost.u-strasbg.fr) (Z. Duputel), [n.fournier@gns.cri.nz](mailto:n.fournier@gns.cri.nz) (N. Fournier).

system (V. Manville, T. Hurst, pers. comm.). After the Crater Lake was re-established, a cyclic pattern of lake temperature fluctuations (~10 month period) occurred. This cyclic pattern was consistent with a heat pipe model proposed by Hurst et al. (1991) and Christenson and Wood (1993), who envisage a shallow convecting magma conduit fluxing heat and gas through the hydrothermal system and into the overlying Crater Lake. Nakagawa et al. (1999) proposed that the shallow volcanic system was composed of magma pockets within a shallow mush zone that was repeatedly injected with new magma prior to the 1995–96 eruption. The Crater Lake level also showed the effects of this temperature cycling, which overprinted the gradually increasing Crater Lake level (i.e., temperature increases promoted lake evaporation). On 4 October 2006 at 22:24 NZDT (09:24 UT), a small eruption occurred within the Crater Lake that produced a 4–5 m-high wave deposit on fresh summit snow (Fig. 1). The eruption onset was marked by a volcanic earthquake ( $2.9 M_L$ ), but produced no airwave and no ash ejection into the atmosphere. It is presumed to have been a small subaqueous eruptive event whose effects were confirmed three days later during a visit to the summit. The explosion was also accompanied by a slow (over 13 days) c. 1.5 m rise of the lake level (Kilgour et al., 2007) which contributed to the 18 March 2007 tephra dam collapse and lahar (Carrivick et al., 2009; Manville and Cronin, 2007).

The Crater Lake was at overflow when the September 2007 eruption occurred. This eruption began at 20:26 NZDT (08:26 UT) with a volcanic earthquake measuring  $3.2 M_L$ . The eruption produced a strong Very-Long Period (VLP) pulse (dominant period of 13 s) and lasted for about 20 s based on airwave pulses observed on two pressure sensors. The eruption was preceded by two small but locatable volcano-tectonic earthquakes at 20:23 NZDT. The eruption

was also preceded by minor tremor episodes at 20:17 NZDT and immediately prior to the main eruption (20:25). This eruption, more powerful than the 2006 event, created a c. 2000 m high steam column above the crater and resulted in a Surtseyan jet which ejected ballistics, ash, lake water and sediments northward on the summit, producing lahars in the Whangaehu and Whakapapaiti catchments (Fig. 1)(Jolly et al. 2010-this issue).

### 3. Interferometry on Retrieved Cross-Correlation Function from Ambient Seismic Noise

Recently, Sens-Schönfelder and Wegler (2006), Brenguier et al. (2008) and Duputel et al. (2009) proposed coupling the theory of Coda Wave Interferometry (CWI) (Poupinet et al., 1984; Snieder, 2006) with passive imaging, using ambient seismic noise, to monitor temporal variations of elastic properties of Mt. Merapi (Indonesia) and Piton de la Fournaise (La Réunion Island). This technique is called IRCCASN in this paper. CWI allows detection of small variations in the mean velocity of scattered waves forming the coda of an earthquake. Several authors have used this technique to monitor volcanoes (Grêt et al., 2005; Ratdomopurbo and Poupinet, 1995) or to detect variations in the Earth's crust due to large earthquakes (Poupinet et al., 1984; Wegler and Sens-Schönfelder, 2007). The main disadvantage with CWI is it needs a repetitive seismic source occurring at the same point to produce waveforms that are as identical as possible before and after a perturbation, so as to be sure that the differences observed are only due to the perturbation and don't reflect changes in the source or path effects. Poupinet et al. (1984) used multiplets, but the source process is not exactly repetitive and their temporal distribution cannot be controlled. Alternatively, Ratdomopurbo and Poupinet (1995) used an artificial source, but this method was expensive and is not practical for most observations. Grêt et al. (2005) used Strombolian explosions of large gas bubbles in the lava lake of Mt. Erebus (Antarctica). Because of the small size of the lake, the location source was well defined and the a posteriori comparison of waveforms showed great similarity, but this configuration cannot be applied on every volcano.

Because of limitations in the source process and temporal dependence on earthquake occurrences, the CWI technique was severely limited until it was coupled with the ambient seismic noise technique. Recent studies have shown that the Green's function (GF), or impulse response, of a medium between two receivers can be rebuilt by cross-correlating a diffuse wave field recorded at these two devices; as if one receiver was an impulsive source and the other recorded this signal. This technique was initially tested in helioseismology to construct images of Sun's internal structure (Duvall et al., 1993). Weaver and Lobkis (2001) applied it in the field of acoustics to show that the thermal noise autocorrelation function was the same waveform as a pulse-echo signal. In seismology, Campillo and Paul (2003) retrieved GFs from the cross-correlation of the coda part of earthquakes, whereas several other studies used the ambient seismic noise (Kang and Shin, 2006; Lin et al., 2007; Shapiro and Campillo, 2004; Shapiro et al., 2005; Stehly et al., 2010). This later technique matches well the aim of volcano monitoring. Indeed, contrary to earthquakes, which are only located in seismogenic zones and have a temporal random occurrence, seismic noise is characterised by a more homogeneous distribution in space and time. Moreover, retrieval of the GF from seismic noise overcomes the bias due to source position and mechanism, allowing continuous and real-time monitoring techniques (Duputel et al., 2009). Recently, Hadziioannou et al. (2009) showed that it was not required to reconstruct Green's functions to monitor accurate temporal changes in seismic velocity but rather to reconstruct stable Cross-Correlation Functions (CCF) in time. Even if the noise sources have a relative unstable distribution, the velocity changes can still be retrieved. Moreover, IRCCASN only needs two seismometers [in fact only one seismometer if the autocorrelation

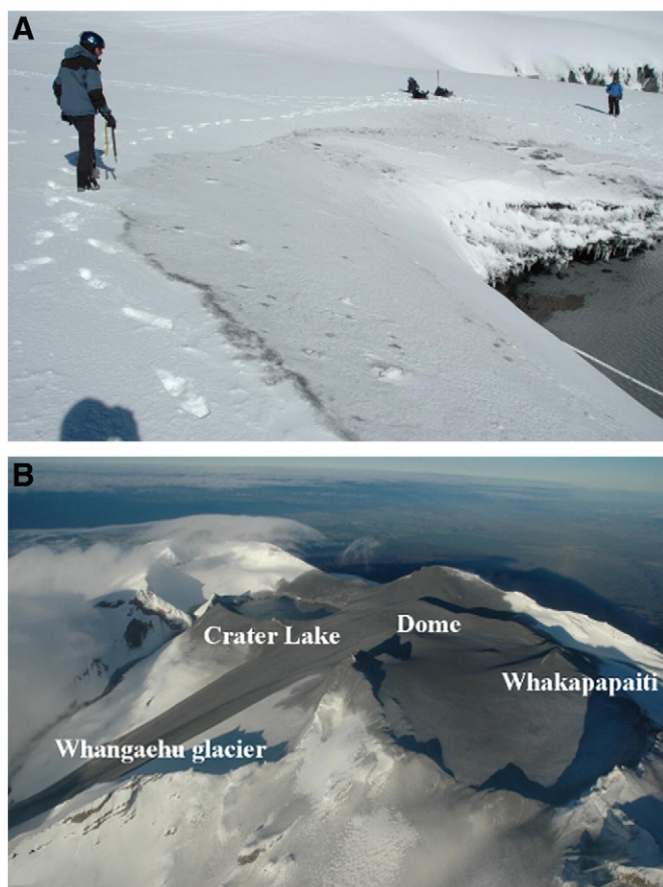


**Fig. 1.** (A) October 2006 eruption. Note the minor deposits left on the Crater Lake edge by the 4–5 m high wave produced by the eruption. (B) September 2007 eruption. Aerial photography from North-East of the Ruapehu summit, the ash deposits and the lahars.

function is used (Wegler and Sens-Schönfelder, 2007)] and thus offers another inexpensive way to monitor a volcano.

#### 4. Data processing

We examined data from 10 short-period seismometers (Sercel L4C-3D, 1 s natural period) and 2 broadband seismometers (Guralp CMG-40T, 60 s natural period) around the edifice of Ruapehu (Fig. 2). To avoid correcting for instrument responses we processed the broadband sensor stations separately from the short-period sensor pairs. However, only the pairs involving NGZ, OTVZ, TUVZ and WNVZ (all short-period) showed significant variations; variations between other pairs were too ambiguous to be absolutely related with the eruption. It would be ideal to numerically reduce the broadband sensor response and increase the number of cross-correlation station pairs. However, we found in limited tests that the relevant station pairs did not produce significant anomalies which would add to our interpretation. Hence we did not proceed with a detailed comparison of all broadband short-period station pairs.

For each station pair, we processed 2 months of data before and after eruptions. We also processed all of 2006 for some relevant pairs but not for all. Data are continuously recorded by the GeoNet network around Ruapehu at a sampling rate of 100 Hz. We followed the method of Brenguier et al. (2008) and Duputel et al. (2009) to retrieve the CCF, using the Z-component for each seismometer. The data were gathered into one day traces. After removing the mean and the trend of the traces, we applied filtering and spectral whitening in the frequency band of 0.2–0.7 Hz, around the second microseism peak

(Stehly et al., 2006). This enabled us to reduce the influence of strong spectral peaks in the noise, such as the strong 2 Hz tremor recorded commonly on Ruapehu (Hurst and Sherburn, 1993). We applied a one-bit normalisation to the data, i.e. we only kept the sign of the raw signal by replacing all positive amplitudes with a 1 and all negative amplitudes with a  $-1$  to avoid the influence of strong amplitude signals like earthquakes. Then, after tapering the traces with a cosine window, we computed 1-minute-long Cross-Correlation Functions in the time domain that we stacked over one day to obtain a daily CCF. This process was applied to each pair of stations.

To observe temporal variations we compared the daily CCFs with a fixed reference. As a Reference CCF, we chose the average CCF computed from 01 April 2007 to 31 August 2007. We chose this period because it was a “quiet” period without eruption or strong tremor. After the cross-correlation computation, both reference and daily CCFs had a causal and an anti-causal side corresponding to the wave travelling from the first station to the second and from the second station to the first, respectively. We normalised each side separately and then averaged them to obtain a 1-minute-long causal CCF. At this stage, the daily CCF’s signal to noise ratio was too low to be properly compared with the Reference CCF. We thus used a stack of the 10 preceding daily CCFs as the Current CCF of the current day (Fig. 3). For a matter of clarity, we call “Current CCF” this stacked CCF. We compared the Current CCF with the Reference CCF using the CWI technique (Hadziioannou et al., 2009; Poupinet et al., 1984; Ratdomopurbo and Poupinet, 1995; Snieder, 2006).

To obtain an estimation of seismic velocity variation, let us consider a reference medium where the seismic wave propagation path is

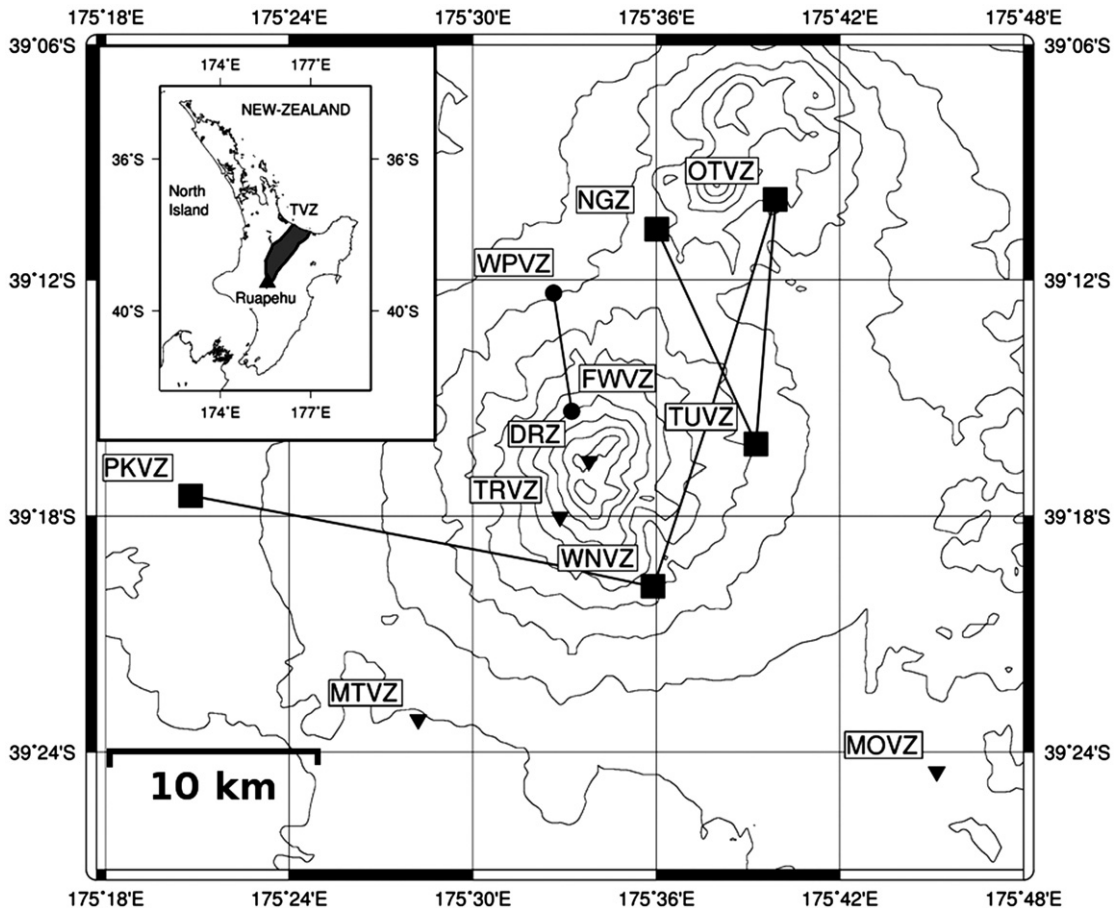
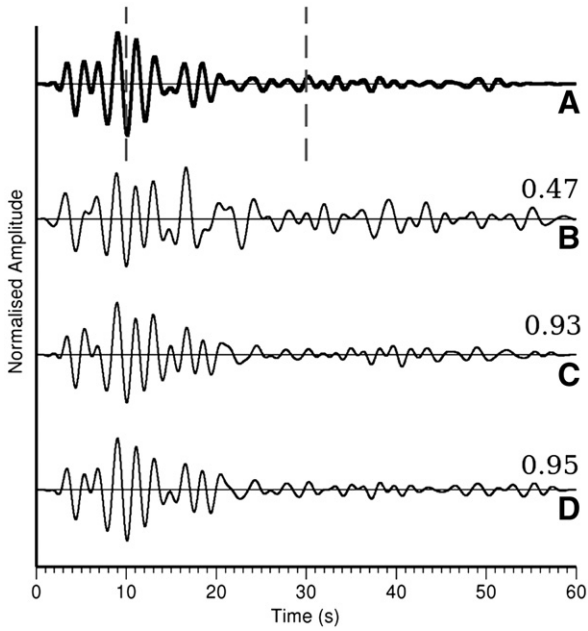


Fig. 2. Location map of Mt. Ruapehu at the southern end of the Taupo Volcanic Zone, North Island, New-Zealand (inset). Map of the GeoNet seismic network around Ruapehu. Short-period seismic stations are shown by reversed black triangles, the seismic stations cited in this study are shown by black squares. The two broadband sensors FWVZ and WPVZ are shown by black circles. Elevation contours are at 200 m intervals. We highlight the paths for the pairs cited in this study. Station TWVZ is out of the map.



**Fig. 3.** From the top to the bottom: (A) in bold, the Reference Cross-Correlation Function (CCF), average of CCFs set along the period from the 01 April 2007 to the 31 August 2007, the gray dashed lines mark the window where the optimization is performed. (B) A raw daily CCF. (C) A Current CCF as a stack of the 5 previous raw daily CCFs. (D) A Current CCF as a stack of 10 previous raw daily CCFs. The three Current CCFs are for the 17th of September 2006. Each curve is normalised by its maximum amplitude. The number on the right is the correlation coefficient between the Reference and the Current CCF for the studied window.

$d = vt$ ,  $d$  being the length of the path,  $v$  the velocity of the seismic wave, and  $t$  the propagation time. If one assumes a homogeneous velocity variation in space  $\delta v$  and if the path is unchanged, then:

$$d = vt = (v + \delta v)(t + \delta t), \tag{1}$$

which gives to first order

$$\frac{\delta v}{v} = -\frac{\delta t}{t} \tag{2}$$

where  $\delta t$  is the propagation time variation induced by the velocity variation. Thus, measuring the relative travel time shift between the Reference CCF and the Current CCF, one can obtain the relative velocity variation.

To measure the relative travel time shift we followed the optimization method of Sens-Schönfelder and Wegler (2006). Recent results (Duputel et al., 2009; Hadziioannou et al., 2009) highlight the stability of this stretching technique when comparing with the moving window cross spectral analysis (Poupinet et al., 1984). We could have applied the stretching analysis separately on the causal and the anti-causal CCF. This would have allowed us to control the symmetry of the stretching coefficient and thus isolate clock problems and other biases as variation in noise sources location. However, we decided to average the causal and anti-causal part of the CCFs to get a better coherency and stability of the reconstructed wave field. We computed a set of 5000 stretched and compressed Reference CCF's according to Eq. (2) with  $\delta t/t$  ranging from  $-3\%$  to  $3\%$ . We used a time window of 10 s to 30 s (Fig. 3A) (4–16 s for the autocorrelation function) to keep only the part of the CCF coda due to coherent strongly scattered waves. Then, for each day, we kept the stretched/compressed Reference CCF that had the largest cross-correlation coefficient with the Current CCF. The daily value of the relative velocity variation  $\delta v/v$  is thus the opposite of the stretching/compressing coefficient. To assess the quality of our inversion, we computed a standard deviation by retrieving  $\delta v/v$  in 4 s non-overlapping time windows ( $i = 1, N$ ) as:

$$E = \sqrt{\frac{\sum_{i=1}^N [(\delta v/v)_i - \delta v/v]^2}{N}} \tag{3}$$

With this technique, we can resolve a relative velocity variation of c. 0.2%.

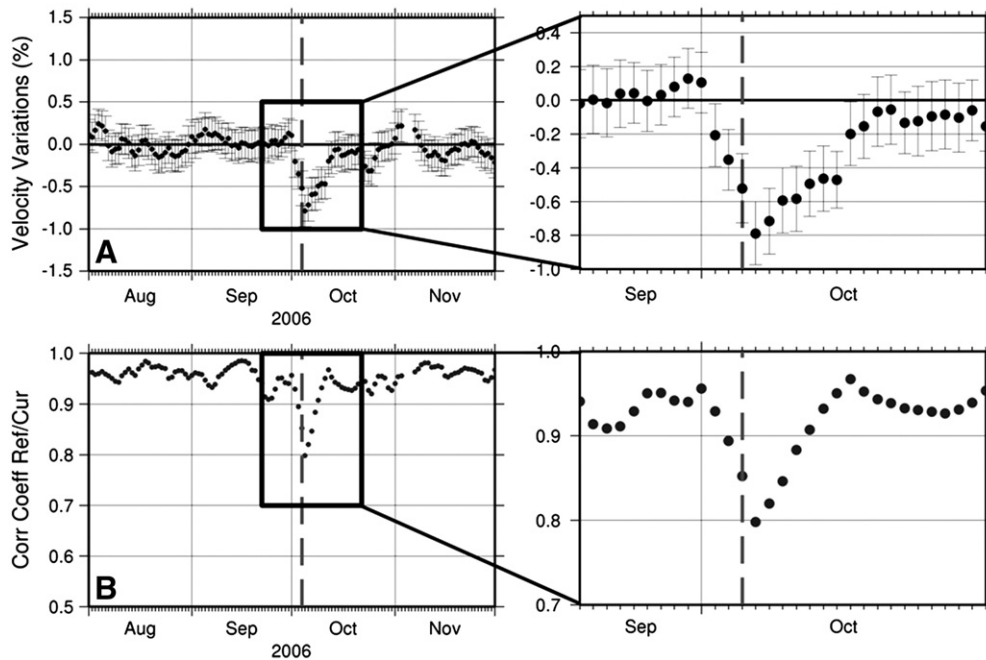


**Fig. 4.** 2006 eruption. (A) Relative seismic velocity variation  $\delta v/v$  between the pair NGZ-TUVZ, the dashed gray line shows the day of the eruption. (B) Cross-correlation coefficients between the Reference CCF and the Current CCF for the pair NGZ-TUVZ. The figures on the right show the enlargement of the 22 September to 22 October period. Note the strong decorrelation which begins 3 days prior to the eruption.

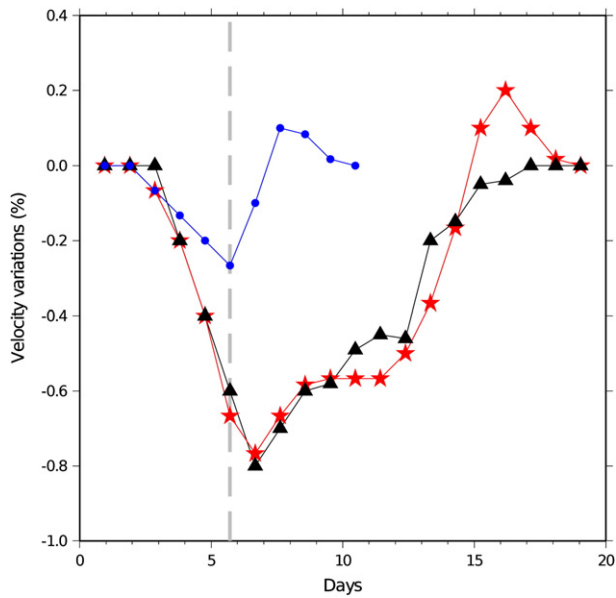


**Fig. 5.** Modelling of the real velocity variations for the 2006 eruption by deconvolving the raw data by a 10-day square window. The black triangles curve is the raw relative velocity variation, the blue dots curve is the modelling of the real velocity variations. The red stars curve is obtained by convolving the real velocity variation model by a 10-day square window.

## 5. Results

We observed significant velocity variations before and after the 2006 eruption. However, no significant variations were observed for the 2007 eruption. We describe the observations for both eruptions in this section, and discuss their significance and the different behaviours of the two eruptions and the different response of the IRCCASN technique in the next section.

### 5.1. 2006 explosion

Fig. 4 shows the result of the optimization for the 2006 event, for the pair NGZ–TUVZ. During the two months before and 40 days after the explosion, the seismic velocity variations were small ( $< \pm 0.25\%$ ). Three days before the explosion, the velocity began to drop, reaching a maximum variation of 0.8% the day after the event. Then, during the next 7 days, the velocity gradually returns to its mean level. The cross-

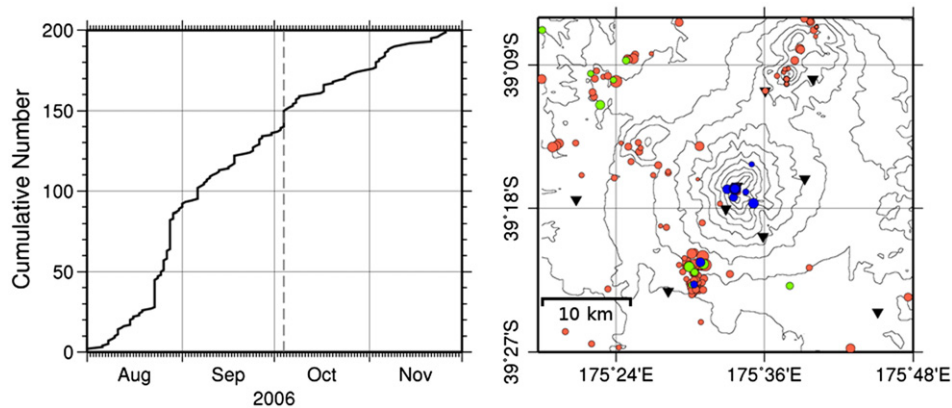
correlation coefficients between the Current CCF and the non-stretched Reference CCF show a strong decorrelation coinciding with the velocity drop (Fig. 4), reaching the mean level at the same time as the velocity. These results show that the process driving this observation is clearly reversible and ephemeral.

The fact that the minima of both the relative velocity (Fig. 4A) and the correlation (Fig. 4B) occur 1 day after the explosion is a result of the 10-day-window averaging, which produces a shift and a stretching of the data toward the future. A simple modelling of the data and a deconvolution by a 10-day-window (Fig. 5) reveal that the velocity minimum actually occurs on the day of the explosion. The velocity started to decrease 3 days before the explosion, reached a minimum velocity on the day of the explosion, and recovered to the long-term average velocity within  $\sim 1$  week.

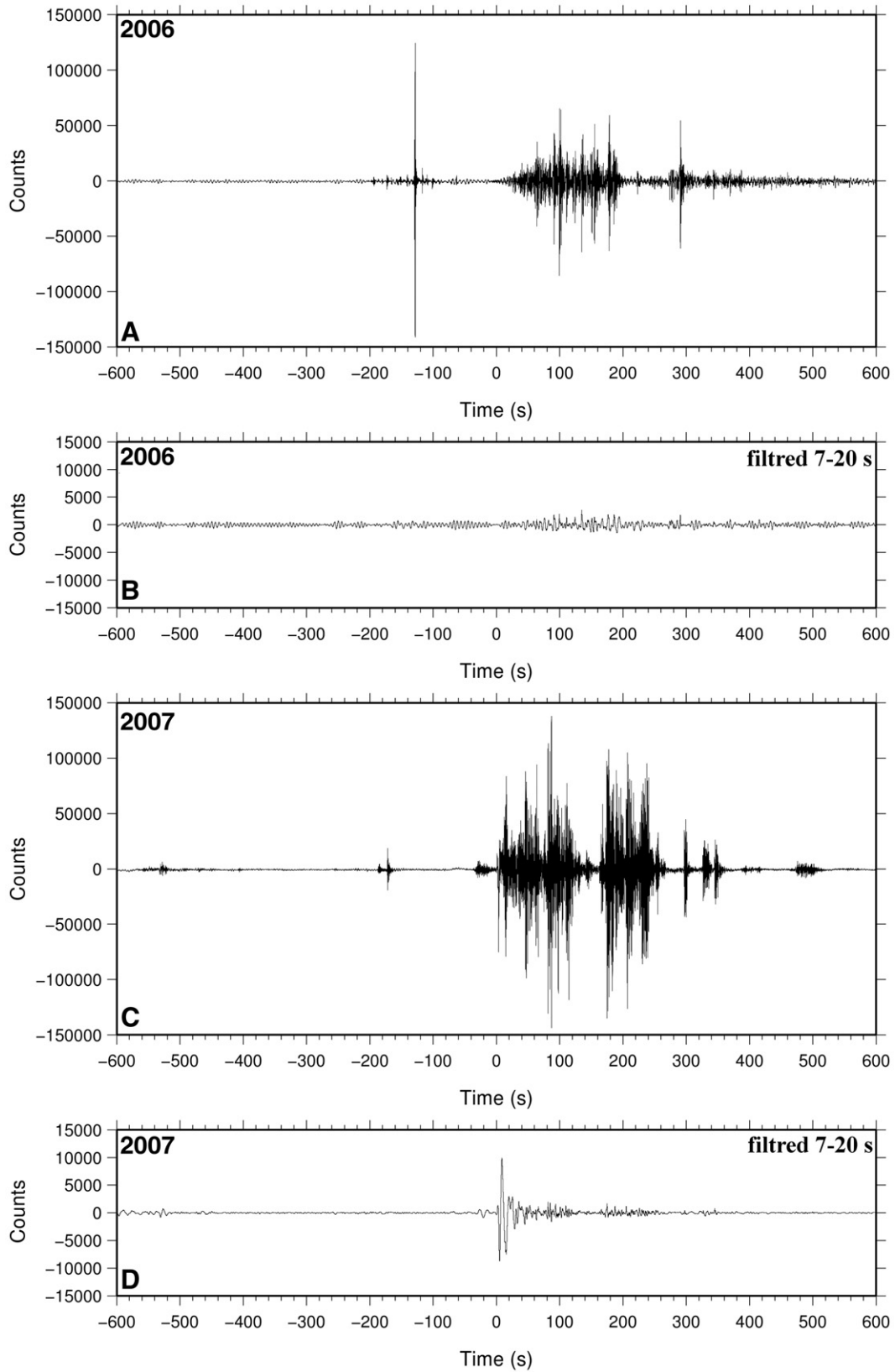
According to Wegler and Sens-Schönfelder (2007), the decorrelation could be caused by two different factors. First, it could be a result of artefacts in processing. By removing the numerous earthquakes and replacing them with zeroes, they reduced the length of their data and so increased the noise level, which created an artificial decorrelation. We applied a one-bit normalisation that produces better results as shown by Bensen et al. (2007). Moreover, earthquakes were uncommon during the two first weeks of October when the changes are observed, principally occurring on the day of the eruption (Fig. 6). The GeoNet catalogue of shallow seismicity ( $< 40$  km) in the studied area shows 23 events for the decorrelation period from 01 October 2006 to 12 October 2006, 11 of which occurred the day of the explosion (Fig. 7). Among these latter earthquakes, nine were volcanic or volcano-tectonic earthquakes, the event at 09:26:23 (all hours in UT) is the record of the explosion. The level of the seismicity between 01 October 2006 and 12 October 2006 is similar to that of the rest of the studied period. Therefore, the decorrelation is probably not caused by a greater number of earthquakes.

Fig. 4B shows the cross-correlation coefficients between the non-stretched Reference CCF and the Current CCFs. The decorrelation is more likely due to the shift created by the disruption  $\delta v/v$  (assumed to be spatially homogeneous) in the medium. However, we also computed the cross-correlation coefficients between the stretched Reference CCF and the Current CCFs which shows the same features (results not shown). This can be the expression of the actual spatial non-homogeneity of  $\delta v/v$  or a slight displacement of the wave scatterers, i.e. the fractures and the heterogeneities in the ground, around the wave path (Snieder et al., 2002; Wegler and Sens-Schönfelder, 2007).

The same behaviour, albeit with a lower velocity drop, was observed on other station pairs (Fig. 8). As the velocity drop is not observed or is too dubious beyond these stations (NGZ, OTVZ, TUVZ



**Fig. 6.** Cumulative number of earthquake of the 01 August to 30 November period (left). Location map of the shallow seismicity ( $< 40$  km) during the studied period. Filled circles show earthquakes, the size of the circle is proportional to the magnitude (the smallest earthquake is  $M_L = 0.679$ , the strongest is  $M_L = 3.085$ ). Black events (blue) are 04 October events, light gray (green) are events from 01 October to 12 October, the period of the velocity drop. Dark gray events (light red) are events for the rest of the studied period. Reverse triangles show stations.



**Fig. 7.** Time sequences of the eruptions recorded at FWVZ. (A) 2006 eruption, raw trace. (B) 2006 eruption, filtered trace (7–20 s). (C) 2007 eruption, raw trace. (D) 2007 eruption, filtered trace (7–20 s) The 4 traces are centred on the onset of each eruption at 09:26 UT and 08:26 UT for the 2006 and 2007 eruption respectively.

and WNVZ), we surmise that the perturbation is likely to be localised on the north-east flank of Ruapehu. Fig. 9 shows data for the pair PKVZ–WNVZ, as example, where no significant variations around the

time of the eruption are observed. It shows also the results for the broadband pair FWVZ–WNVZ, which are quite ambiguous. For this pair we find an increase of the velocity of ~0.4% and a strong

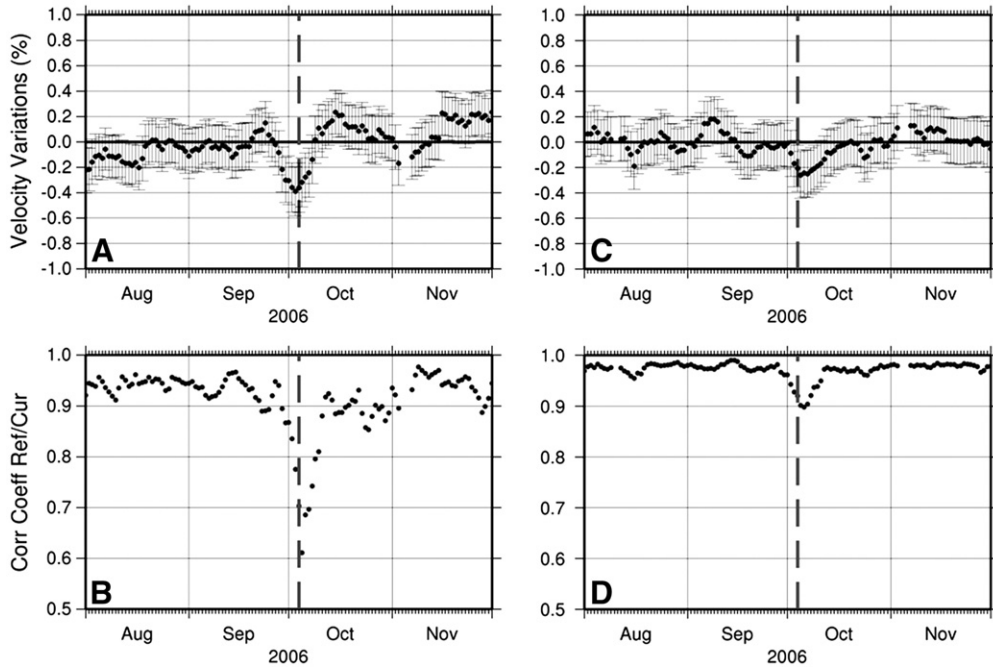


**Fig. 8.** 2006 eruption. (A) Relative seismic velocity variation  $\delta v/v$  between the pair OTVZ-TUVZ, the dashed gray line shows the day of the eruption. (B) Cross-correlation coefficients between the Reference CCF and the Current CCF for the pair OTVZ-TUVZ. (C) and (D): the same as (A) and (B) but for the couple OTVZ-WNVZ. Note the different sensitivity of the cross-correlation coefficient for each pair, the same variations are recorded at both pairs but the amplitudes are different.

decorrelation. However, if we consider the whole 2006 year (Fig. 10) we find that these velocity variation and decorrelation patterns are common for this station pair and might not reflect volcanic processes.

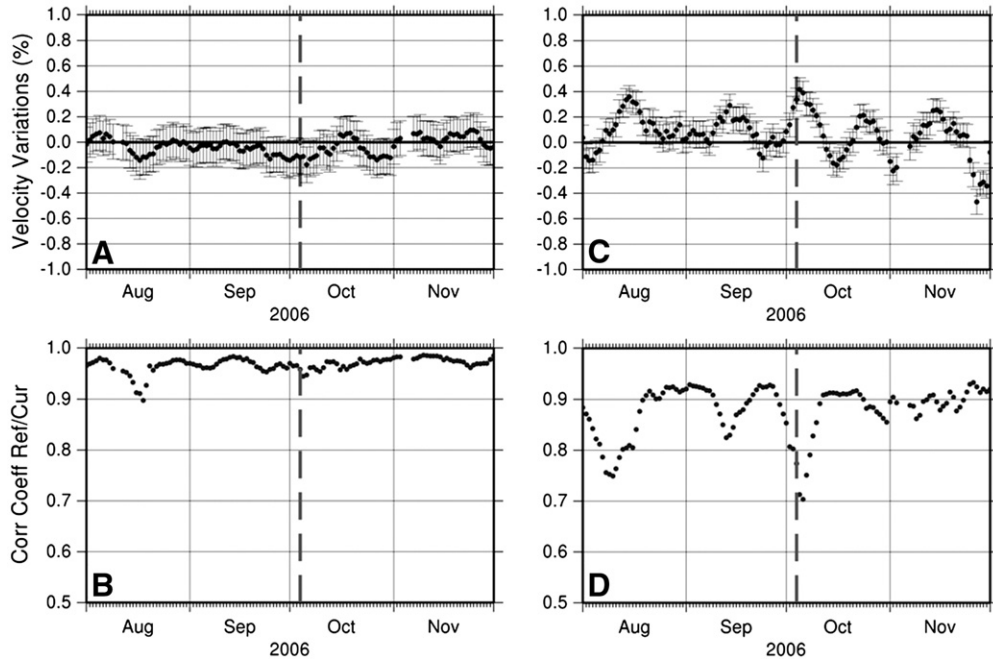
5.2. 2007 eruption

Fig. 11 shows the results for the 2007 eruption for two pairs we used for the 2006 eruption: NGZ-TUVZ and OTVZ-WNVZ. No significant change is observable around the 25 September eruption.

A small decorrelation occurred around the onset of the eruption (Fig. 11B, D), without any associated velocity variation. These results are too uncertain to be interpreted as effects due to volcanic activity.

6. Discussion

The long-term results for 2006 (Fig. 10) show several velocity variations. We observe a clear drop on the onset of the eruption for some station pairs but we also observe long-period variations overprinting



**Fig. 9.** 2006 eruption. (A) Relative seismic velocity variation  $\delta v/v$  between the pair PKVZ-WNVZ, the dashed gray line shows the day of the eruption. (B) Cross-correlation coefficients between the Reference CCF and the Current CCF for the pair PKVZ-WNVZ. (C) and (D): the same as (A) and (B) but for the couple FWVZ-WPVZ.

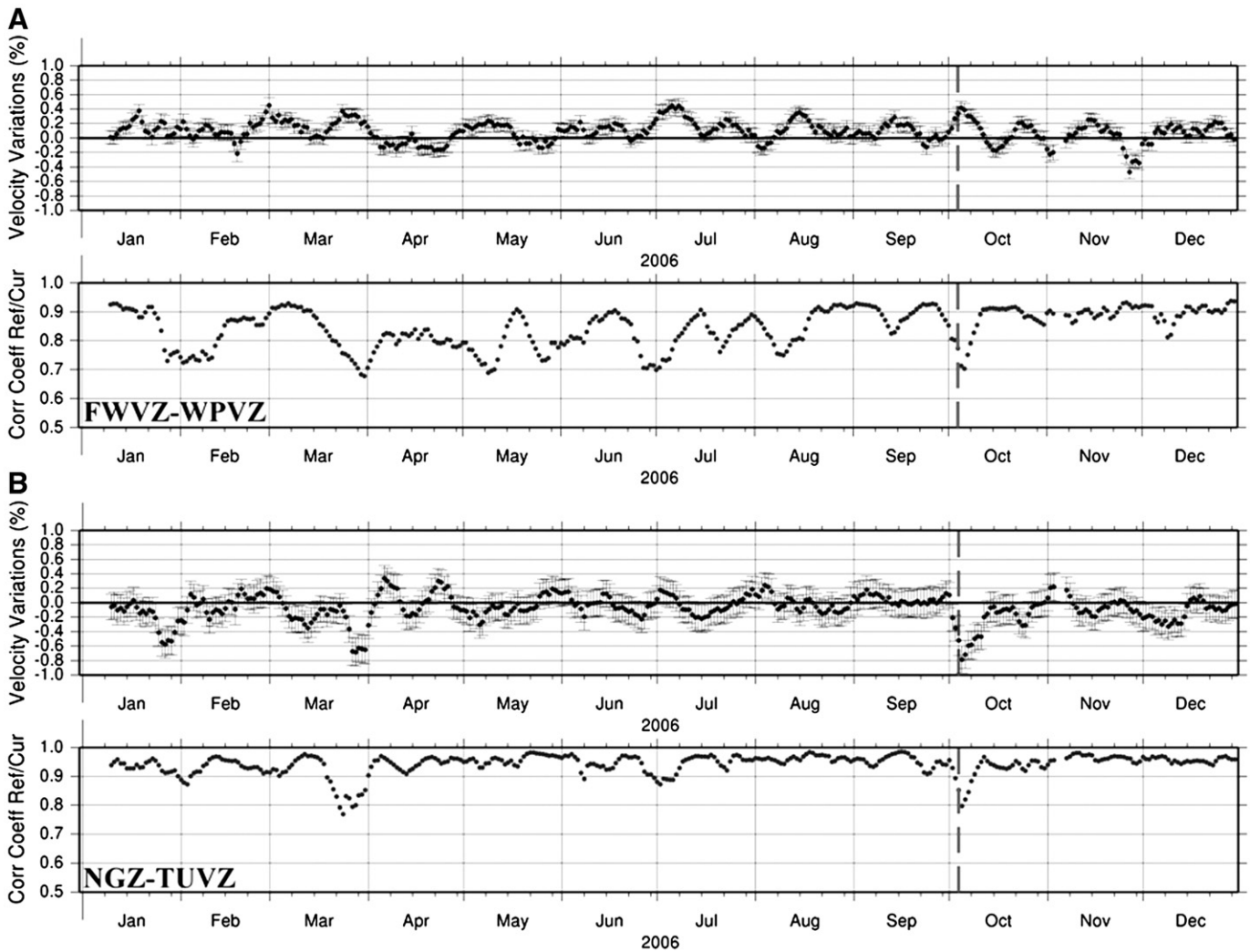


**Fig. 10.** 2006 eruption. (A, top) Relative seismic velocity variation  $\delta v/v$  between the pair FWVZ-WPVZ for the year 2006, the dashed gray line shows the day of the eruption. (A, bottom) Cross-correlation coefficients between the Reference CCF and the Current CCF for the pair FWVZ-WPVZ. (B, top) and (B, bottom): the same as (A, top) and (A, bottom) but for the couple NGZ-TUVZ. The eruption is not obviously recorded for FWVZ-WPVZ and the results remain ambiguous. The decorrelation in March for NGZ-TUVZ is due to a strong storm above NGZ which created noise and prevented the proper retrieval of the CCF.

the drop associated with the eruption. These long-period ( $\sim 1$  month) variations are observed at most of station pairs. Such velocity variations have also been observed at La Réunion by Brenguier et al. (2008). We compared these variations with theoretical vertical ground motion due to the Earth tides at Ruapehu (Milbert, 2008), but no clear correlation was observed (Fig. 12). The Crater Lake temperature also is not correlated with the long-term velocity variations. In 2006/2007, Crater Lake temperature varied with 9–10 months period (Fig. 12). Comparisons between our IRCCASN and observed lake temperatures suffer from low sampling rates for the temperature data and insufficient seismic network prior to 2006. Such a study will be more feasible in the future as high sample rate automated temperature datasets which have recently been established mature (Hurst, pers. comm.).

The velocity drop and associated decorrelations seen in March 2006 (Fig. 10) and in the middle of August 2007 (Fig. 11) are probably related to strong storm systems. Indeed, the wind and the rain during these heavy weather episodes produced a high level of noise which decreased the seismic signal quality and the signal-to-noise ratio, resulting in more ambiguity in construction of the Current CCFs. Velocity variation artefacts are produced due to inversion of distorted Current CCFs.

Such variations could also be caused by artefacts due to instrumental timing errors. We addressed this possibility by computing the autocorrelation function for station TUVZ (Fig. 13). Although noisier,

we still found similar changes in velocity as described above. Thus, an instrumental timing shift cannot be responsible for the variations seen at Ruapehu.

The strong 2 Hz tremor common at Ruapehu might also have an influence on the decorrelation. Indeed, if the tremor source is not stationary in time, the effect of this migrating source could be confused for a velocity variation in the medium. However, the data processing (spectral whitening and filtering between 0.2 and 0.7 Hz, see Section 4 Data Processing) strongly decrease the influence of tremor. Moreover, Fig. 14 shows that even if there had been strong tremor starting a few days before the eruption, which could produce a decorrelation, there was also strong tremor at the beginning of September which did not produce any significant variations (arrow in Fig. 14).

To assess the influence of a CCF decorrelation on velocity variation measurements we performed a synthetic test by adding noise to a Reference CCF. We computed the error on the velocity variation measurement which is a function of the signal-to-noise ratio (SNR). For a white Gaussian noise of zero mean and  $\sigma^2$  variance,

$$SNR_j = \frac{\sum_{i=1}^N S_i^2}{N\sigma_j^2} \quad (4)$$

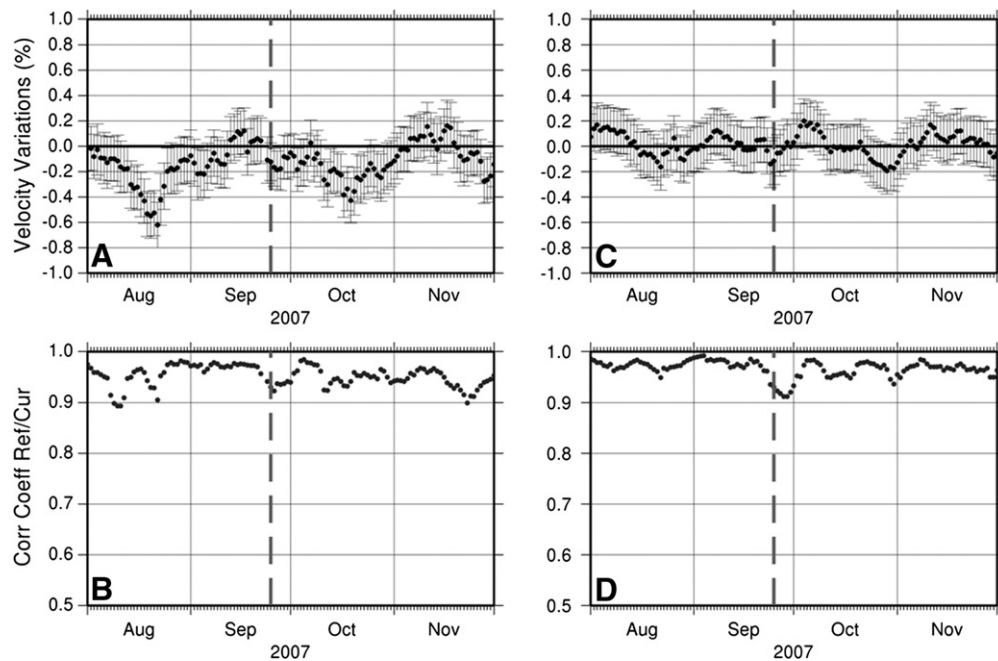


**Fig. 11.** 2007 eruption. (A) Relative seismic velocity variation  $\delta v/v$  between the pair NGZ-TUVZ, the dashed gray line shows the day of the eruption. (B) Cross-correlation coefficients between the Reference CCF and the Current CCF for the pair NGZ-TUVZ. (C) and (D): the same as (A) and (B) but for the couple OTVZ-WNVZ.

with  $N$  being the number of samples in the signal  $S$ , here the Reference CCF, and  $\sigma$  varying from 0.01 to 1 by 0.01 steps. Fig. 15 shows that even if there is a high level of noise in the Reference CCF, most of time the error on the velocity variation stays under 0.25%, in the error bars. Moreover, for a  $\text{SNR} > 3$  dB, i.e. for a  $2 \times \text{SNR}$ , the velocity variation measurement remains stable. The same pattern was observed when we added noise to the Current CCF instead of the Reference CCF. This shows that the stretching method is very robust (Hadziioannou et al., 2009) even for noisy CCFs. We conclude that the velocity variations seen during the 2006 eruption were not an artefact associated with the CCFs decorrelation.

These examples reveal common pitfalls of the IRCCASN method. Many artefacts can arise from non-volcanic phenomena, and several factors can affect the velocity variation computation leading to potentially incorrect interpretations. At Ruapehu we have demonstrated that such pitfalls do not significantly affect our results, and that the observed changes are attributable to localised velocity variations beneath the NE flank of Ruapehu during the 2006 eruption. Such velocity variations are not observed associated with the 2007 eruption however.

In a similar study, Brenguier et al. (2008) and Duputel et al. (2009) reported a similar drop in seismic velocity before eruptions at Piton de la Fournaise (La Réunion Island). They interpret these velocity drops to reflect the opening of cracks during a pre-eruptive inflation period of the edifice caused by an overpressure in a shallow magmatic chamber.

To understand the process that might produce the observations at Ruapehu, we must consider: 1) the time scale of the observations, 2) the location of observed velocity changes on the NE flank of Ruapehu, 3) the observed deposits and 4) changes in the hydrothermal system and Crater Lake.

The observed velocity changes in October 2006 are linked to a small subaqueous eruption which produced a 1.5 m increase in lake level (equivalent to  $3 \times 10^5 \text{ m}^3$ ) but no surface expression of magma. The observed velocity change was localised on the NE flank of the volcano and lasted  $\sim 1$  week. Hence it was much shorter in duration than the observed stress changes associated with the 1995–96 eruption of Ruapehu (Gerst and Savage, 2004; Miller and Savage,

2001), which lasted for several years in the shallow crust and continue to modify the deep velocity structure. The 2006 eruption is also fundamentally different from the 2007 eruption; the 2006 eruption produced only minor changes to the shallow hydrothermal system (a minor long-term increase in  $\text{CO}_2$  and  $\text{SO}_2$ ), while the 2007 event produced substantial changes, including shallow tremor and increased degassing which lasted for several months. Why did the October 2006 eruption produced a localised velocity change while the 2007 event did not?

The results suggest that stress perturbations, and attendant velocity changes, operate over different time scales at different depths and eruptive scales. The 1995–96 Ruapehu eruption introduced sufficient magma to perturb the stress over a wide area and depth range because it was larger, the amplitude of the stress changes were greater, and the stress perturbation dissipated more slowly. The 2006 eruption must have produced a small stress perturbation, which was localised on the NE flank of the volcano, and dissipated within a few days of the eruption. The 2007 eruption might have produced stronger stress perturbations but also of much shorter duration, such that they were not observed using the IRCCASN method. Instead the stress perturbations for the 2007 eruption could have dissipated within a few hours of the eruption or been so localised that they were not observed at any local station pairs.

The 2006 eruption could have resulted from a localised flux of a gas and/or magma through a shallow ( $\sim 3$  km) resident magmatic mush zone at Ruapehu (Nakagawa et al., 1999) (Fig. 16). The gas/magma pocket may have produced a steady increase in pressure until the pressure exceeded the tensile strength of the overlying magma carapace and then began to release fluids towards the surface. As the fluid pulse propagated to the surface it may have reduced the effective stress on fractures near the surface (the observed VT earthquakes before the eruption) (Fig. 7). The fracturing then increased the permeability leading to localised depressurization and the subaqueous eruption. The slow ( $\sim 7$  days) return of the velocity to long-term background levels might be due to slow equilibration of shallow cracks into the unsealed magma carapace. We surmise that the 2007 eruption occurred due to a similar gas/magma flux. The new open volcanic system slowly degassed until a fresh pocket of gas/magma entered the

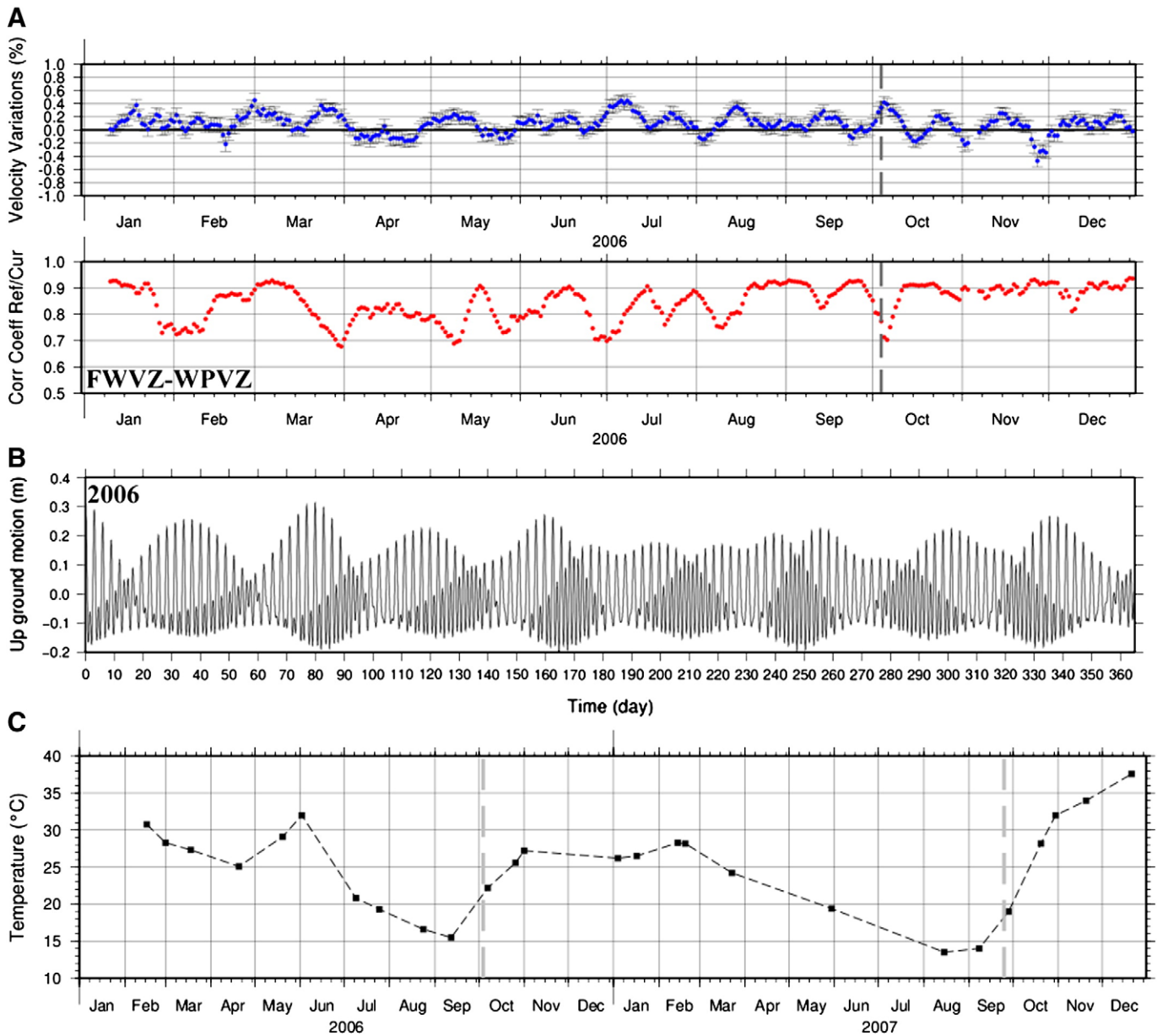


Fig. 12. Comparison between the long-period velocity variations and correlation for 2006 at station pair FWVZ-WPVZ (A), the theoretical up ground motion at Ruapehu created by the solid Earth tides for 2006 (B) and the Crater Lake temperature variations along 2006 and 2007 (C).

magma chamber on the 25 September 2007. Because the system was “open” it did not follow the same pressurization/depressurization cycle observed by IRCCASN in October 2006. Instead the gas slug proceed rapidly to the surface (expressed as a VLP pulse and shallow tremor) (Fig. 7) producing the observed eruption (Jolly et al., 2010-this issue). This model is consistent with the observed pre-eruption VLP signal, gas geochemistry, and also evidence for juvenile magma found in 25 September eruption deposits (Christenson et al., 2010-this issue; Kilgour et al., 2010-this issue). It is interesting to note that for both eruptions volcano-tectonic earthquake activity occurred c. 150 s before the onset of the eruption. We surmise that both sequences were the result of either a failure of magma carapace/hydrothermal seal or the entrance of fluids in the hydrothermal system that acted on localised fractures.

Our model is consistent with a previous study of the Tongariro Volcanic Center done by Rowlands et al. (2005) which shows that low velocities from tomography are centred about 4–5 km to the east of the summit and 5 km depth. In addition, Ingham et al. (2009) showed

that a high conductivity zone exists northeastward from Ruapehu to 8 km depth based on magneto-telluric observations. They interpreted this feature as “the volcanic conduit by which hot volcanic fluids and, potentially, magma are transported to the volcanic cones” (Ingham et al., 2009).

This raises the issue of whether or not such pressure changes at the aforementioned location would not be expected to produce any detectable ground deformation. In other words, is such pressure source consistent with the lack of ground deformation recorded at the various GPS stations at – and around – Ruapehu?

#### 6.1. Pressure changes and associated deformation

To examine whether the pressure changes inferred from the velocity variations may induce detectable ground deformation, we first estimate the overpressure at depth and then assess the resulting ground deformation through simple point source Mogi models.

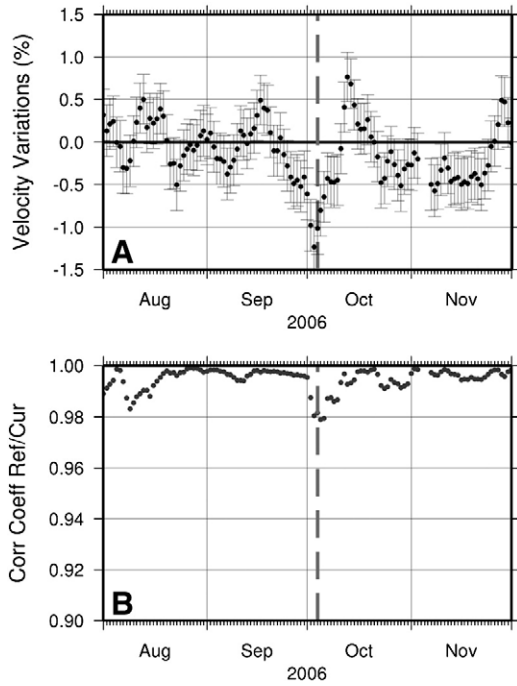


**Fig. 13.** 2006 eruption. (A) Relative seismic velocity variation  $\delta v/v$  inverted from the autocorrelation function using station TUVZ, the dashed gray line shows the day of the eruption. (B) Cross-correlation coefficients between the Reference CCF and the Current CCF for the autocorrelation function using station TUVZ. Note the very high values of cross-correlation coefficients.

Waves velocities can be expressed as

$$V_p = \sqrt{\frac{\kappa + \frac{4}{3}\mu}{\rho}}, \quad (5)$$

$$V_s = \sqrt{\frac{\mu}{\rho}}, \quad (6)$$

and

$$\frac{V_p}{V_s} = 1.73 \quad (7)$$

with Eq. (7) from Hurst and McGinty (1999) for Ruapehu and  $V_p = 4200 \text{ m s}^{-1}$ .

Assuming a density  $\rho$  of  $\sim 2200 \text{ kg m}^{-3}$ , we obtain a shear modulus  $\mu$  of  $\sim 13 \text{ GPa}$  and a bulk modulus (incompressibility factor)  $\kappa$  of  $\sim 22 \text{ GPa}$ . Using a classical model of dilatancy (Brenquier et al., 2008),

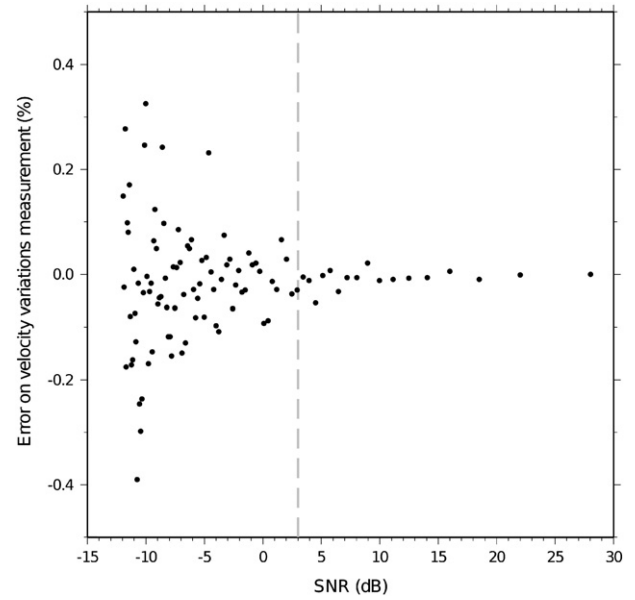


**Fig. 15.** Error on velocity variation measurement function of the signal-to-noise ratio of a synthetic noisy Reference CCF. A white Gaussian noise with zero mean and standard deviation ranging from 0.01 to 1 was added. Note the stability of the velocity variation measurement above 3 dB.

we can link velocity changes  $\frac{\Delta\beta}{\beta}$  to the pressure change  $\Delta P$  and bulk porosity  $\varphi$  as follows:

$$\frac{\Delta\beta}{\beta} = -\frac{1}{2} \frac{\Delta P}{\kappa\varphi}. \quad (8)$$

From ambient noise analysis,  $\frac{\Delta\beta}{\beta_{\text{max}}}$  is  $\sim -0.8\%$ . Assuming  $\varphi \sim 0.1$  (Brenquier et al., 2008) and  $\kappa$  as above, we obtain a pressure change  $\Delta P_{\text{max}}$  of  $\sim 34 \text{ MPa}$ .

Ground surface displacement  $u$  caused by a tension-sphere source in a homogeneous half-space (Lu et al., 2002; Mogi, 1958) can be expressed as follows in a Cartesian system:

$$u_i(x_1 - x'_1, x_2 - x'_2, -x_3) = C \frac{x_i - x'_i}{|R|^3} \quad (9)$$

with  $x_i$  the location of the point of interest at the free surface ( $x_1$ ,  $x_2$  and  $x_3 = 0$  the easting, northing and elevation respectively). Similarly,  $x'_i$  is the location of the source with  $x'_1$ ,  $x'_2$  and  $-x'_3$  the easting, northing and the depth ( $x'_3$  positive) of the source respectively.  $C$  is a combination of material properties and source strength and  $R$  is the distance between the source and the points at which displacement is calculated (Lu et al., 2002). Reformulating these

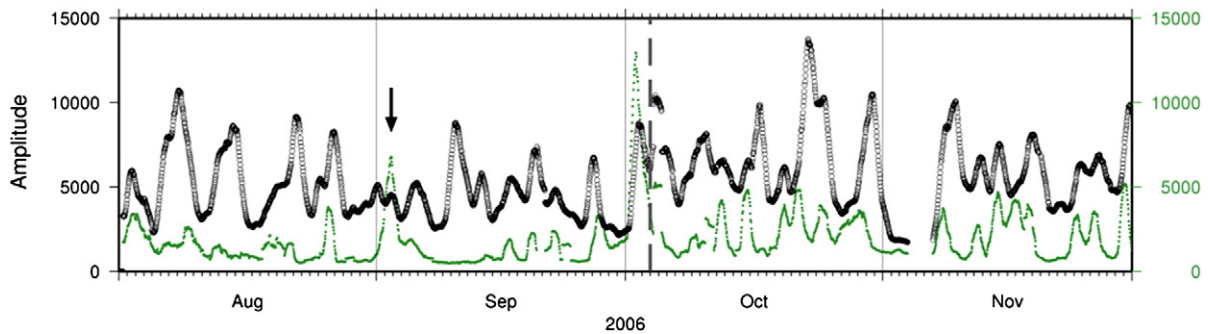


**Fig. 14.** Volcanic tremor measured at TUVZ for the 1.8 Hz–2.3 Hz band (gray points, green points on the online version). Amplitude of the 0.2–0.7 Hz band used to compute the Cross-Correlation Functions (black circles). The two curves are plotted with the same scale. The arrow shows a strong tremor period.

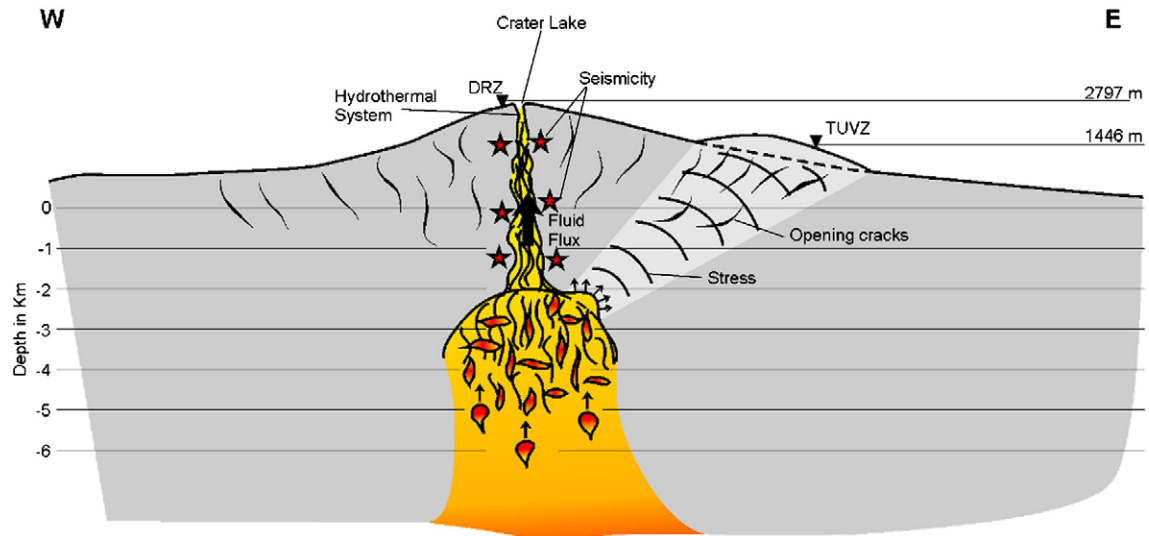


Fig. 16. Conceptual model for the 2006 eruption. The vertical and horizontal scale are identical.

equations for  $x_0$ ,  $y_0$  and  $d$  the source location (easting, northing and depth respectively), 3D modelled displacements  $U$  at the nodes of coordinates  $(x, y, z=0)$  on a flat, free surface grid (in metres) can be rewritten as:

$$U(x, y, z) = \begin{bmatrix} C(x-x_0) \\ C(y-y_0) \\ Cd \end{bmatrix}. \quad (10)$$

In the case of a Mogi source (Mogi, 1958)

$$C = \Delta P(1-\nu) \frac{a^3}{\mu} = \Delta V \frac{(1-\nu)(1+\nu)}{2\pi(1-2\nu)} \quad (11)$$

with  $\nu$  the Poisson's ratio (assumed here to be 0.25),  $a$  the source radius and  $\Delta V$  the volume change inside the spherical source (i.e., volume of magma entering the reservoir).

Note the non-unicity of the results with the intrinsic link between the spherical source radius  $a$  and the overpressure  $\Delta P$  in (i.e., great pressure in a small source cannot be distinguished from a smaller overpressure in a larger source). It follows that if the pressure and location of the source is known, though, one can estimate the radius of the pressure source as well as the volume  $\Delta V$  of material intruded inside the reservoir.

No ground deformation was detected prior to the 2006 and 2007 eruptions with the GeoNet GPS network in the Tongariro National Park. We used this relation between  $\Delta P$  and  $a$  to assess the maximum size of a 5-km deep source with an overpressure  $\Delta P$  of 34 MPa, catering for the observed lack of ground deformation. Two source locations were tested:

- (1) Centred on the active crater: ( $x_0 = 2,731,269$  m,  $y_0 = 6,210,494$  m,  $d = 2500$  mbsl) in the NZMG geodetic system (source 1 in Fig. 17).
- (2) Off-centred to the North East of the active crater: ( $x_0 = 2,733,740$  m,  $y_0 = 6,216,200$  m,  $d = 2500$  mbsl) (source 2 in Fig. 17).

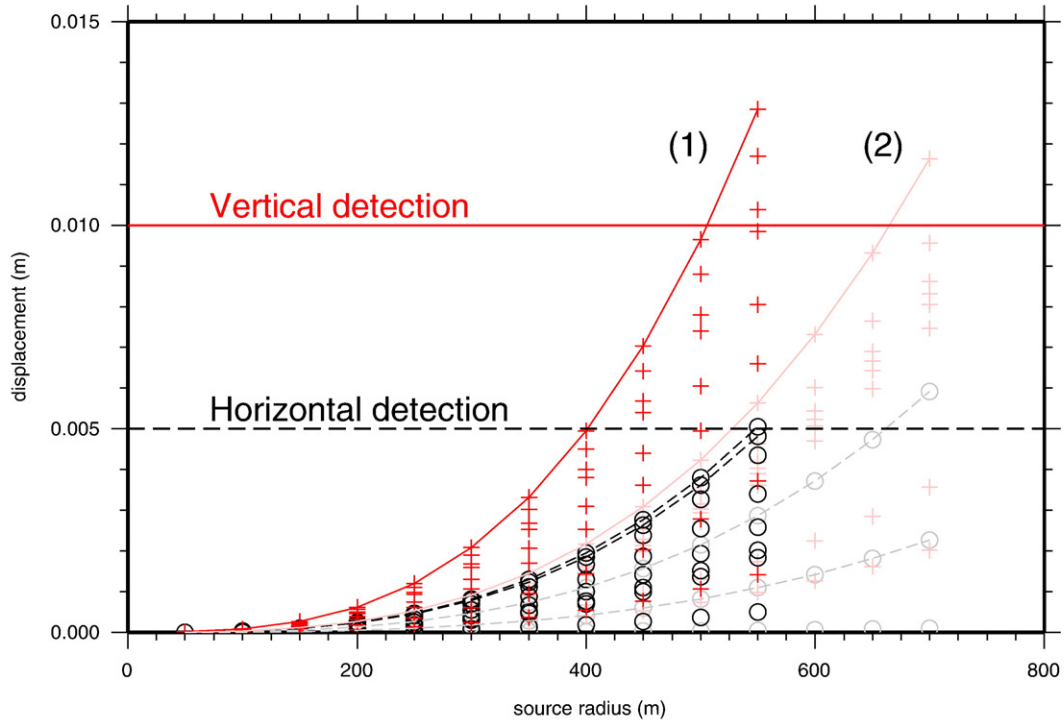
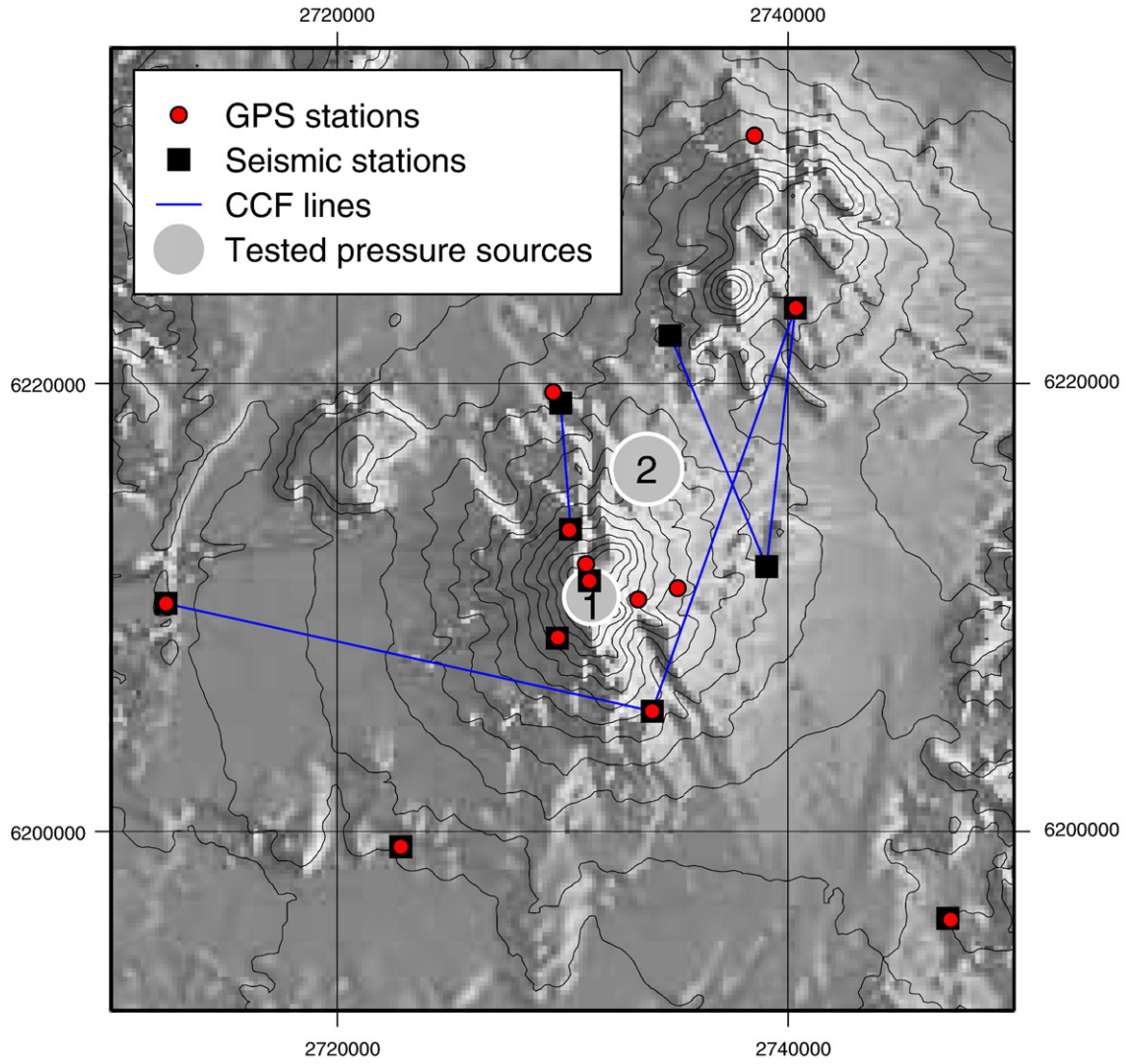
In both cases,  $\Delta P = 34$  MPa, depth  $\sim 5$  km below the summit (i.e., 3.5 km below sea level). Taking a GPS detection limit of 5 mm and 10 mm horizontally and vertically respectively, Mogi models were run for a range of increasing source radii till any of the modelled displacements at the GPS stations became virtually detectable.

The maximum radius for which for a simple Mogi source at 5 km depth and  $\Delta P$  of 34 MPa would remain undetected is  $\sim 550$  m when the source is located below the active vent, and  $\sim 700$  m if the source is offset to the North East (Fig. 17). Putting these results in terms of volume change at the source, we obtain corresponding  $\Delta V$  of magma entering the reservoir of  $\sim 0.8 \times 10^6$  m<sup>3</sup> (or 0.0008 km<sup>3</sup>) and  $1.7 \times 10^6$  m<sup>3</sup> (or 0.0017 km<sup>3</sup>) respectively.

Previous works (Ingham et al., 2009; Rowlands et al., 2005) suggested the presence of small magma bodies near 5 km depth, both under the active vent and 4–5 km NE from the crater. This is consistent with the limited maximum size of the pressure source inferred from the IRCCASN, a simple Mogi point source approach and the lack of ground deformation prior to these eruptive events. From a deformation standpoint, a centred and an offset pressure sources are equally plausible and cannot be discriminated.

## 7. Conclusion

It has been shown that the IRCCASN technique can be applied for volcano monitoring of large basaltic systems like Piton de la Fournaise (Duputel et al., 2009). We are presently testing this method as a possible monitoring tool on active composite cone volcanoes like Ruapehu. The method reveals statistically significant velocity changes that we infer are a result of local volcanic processes occurring prior to eruptive activity. Hence the method can be incorporated into monitoring at Ruapehu to test its applicability for eruption forecasting. We interpret the October 2006 velocity drop as a pressure increase in a small magma reservoir at depth beneath the NE flank of Ruapehu due to the intrusion of small amount of magma (maximum volume of 0.0017 km<sup>3</sup>, or  $\sim 0.1\%$  of the volume of the corresponding reservoir). This is, in turn possibly led to some limited cracks opening above it. While some similarities between the 2006 and 2007 eruption lead us to believe that the same processes occurred prior to both eruptions, one cannot be conclusive about the 2007 event since any pressure change may have fallen below the temporal detection limit of IRCCASN. Furthermore, more work is needed on the small velocity changes observed between periods of activity to determine whether they are linked to environmental factors [e.g. rainfalls or atmospheric pressure changes (Sens-Schönfelder and Wegler, 2006; Niu et al., 2008)] or whether they can be attributed to subtle – yet insofar undetected – changes in volcanic activity at Mt. Ruapehu.



## Acknowledgments

This research was partially funded by the Geologic Hazards and Society-Foundation for Research Science and Technology (GHS-FRST) CO5X0804 and used data from the GeoNet project. Maps and figures were generated with Generic Mapping Tools (Wessel and Smith, 1998). We like to thank Geoff Kilgour, Steve Sherburn, Bill Fry and Tony Hurst for their advice and the careful proofreading they made on a previous version of the manuscript; B. Christenson for the idea that intrusion caused the long-term degassing trends after 2007 eruption. We acknowledge Seth Moran and an anonymous reviewer for the comments which improved this manuscript. Broadband seismometers used in this study were provided by DoC, short-period seismic and GPS data by GeoNet and EQC who are gratefully acknowledged.

## References

- Bibby, H.M., Caldwell, T.G., Davey, F.J., Webb, T.H., 1995. Geophysical evidence on the structure of the Taupo Volcanic Zone and its hydrothermal circulation. *J. Volcanol. Geotherm. Res.* 68, 29–58.
- Bensen, G.D., Ritzwoller, M.H., Barmin, M.P., Levshin, A.L., Lin, F., Moschetti, M.P., Shapiro, N.M., Yang, Y., 2007. Processing seismic ambient noise data to obtain reliable broad-band surface wave dispersion measurements. *Geophys. J. Int.* 169, 1239–1260.
- Brenguier, F., Shapiro, N.M., Campillo, M., Ferrazzini, V., Duputel, Z., Coutant, O., Nercessian, A., 2008. Toward forecasting volcanic eruptions using seismic noise. *Nature Geosciences* 1, 126–130.
- Bryan, C.J., Sherburn, S., 1999. Seismicity associated with the 1995–1996 eruptions of Ruapehu volcano, New Zealand: narrative and insights into physical processes. *J. Volcanol. Geotherm. Res.* 90, 1–18.
- Bryan, C.J., Sherburn, S., 2003. Eruption-induced modifications to volcanic seismicity at Ruapehu, New Zealand, and its implications for eruption forecasting. *Bull. Volcanol.* 65, 30–42.
- Campillo, M., Paul, A., 2003. Long-range correlations in the diffuse seismic coda. *Science* 299, 547–549.
- Carrivick, J.L., Manville, V., Cronin, S., 2009. Modelling the March 2007 lahar from Mt Ruapehu. *Bulletin of Volcanology* 71 (2), 153–169. doi:10.1007/s00445-008-0213-2.
- Christenson, B.W., Wood, C.P., 1993. Evolution of a vent-hosted hydrothermal system beneath Ruapehu Crater Lake, New Zealand. *Bull. Volcanol.* 55, 547–565.
- Christenson, B.W., Reyes, A.G., Young, R., Moebis, A., Sherburn, S., Cole-Baker, J., Britten, K., 2010. Cyclic processes and factors leading to phreatic eruption events: insights from the 25 September 2007 eruption through Ruapehu Crater Lake, New Zealand. *J. Volcanol. Geotherm. Res.* 191, 15–32.
- Duputel, Z., Ferrazzini, V., Brenguier, F., Shapiro, N., Campillo, M., Nercessian, A., 2009. Real time monitoring of relative velocity changes using ambient seismic noise at the Piton de la Fournaise Volcano (La Réunion) from January 2006 to June 2007. *J. Volcanol. Geotherm. Res.* 184, 164–173. doi:10.1016/j.jvolgeores.2008.11.024.
- Duvall, T., Jefferies, S., Harvey, J., Pomerantz, M., 1993. Time distance helioseismology. *Nature* 362, 430–432.
- Gerst, A., Savage, M.K., 2004. Seismic anisotropy beneath Ruapehu Volcano: a possible eruption forecasting tool. *Science* 306, 1543–1547.
- Grêt, A., Snieder, R., Aster, R.C., Kyle, P.R., 2005. Monitoring rapid temporal changes in a volcano with Coda Wave Interferometry. *Geophys. Res. Lett.* 32, L06304.
- Hackett, W.R., Houghton, B.F., 1989. A facies model for a Quaternary andesitic composite volcano: Ruapehu, New Zealand. *Bull. Volcanol.* 51, 51–68.
- Hadziioannou, C., Larose, E., Coutant, O., Roux, P., Campillo, M., 2009. Stability of monitoring weak changes in multiply scattering media with ambient noise correlation: laboratory experiments. *J. Acoust. Soc. Am.*
- Hurst, A.W., McGinty, P., 1999. Earthquake swarms to the west of Mt Ruapehu preceding its 1995 eruption. *J. Volcanol. Geotherm. Res.* 90 (1–2), 19–28.
- Hurst, A.W., Sherburn, S., 1993. Volcanic tremor at Ruapehu: characteristics and implications for the resonant source. *N.Z. J. Geol. Geophys.* 36, 475–485.
- Hurst, A.W., Bibby, H.M., Scott, B.J., McGuinness, M.J., 1991. The heat source of Ruapehu Crater Lake; deductions from the energy and mass balances. *J. Volcanol. Geotherm. Res.* 46, 1–20.
- Ingham, M.R., Bibby, H.M., Heise, W., Jones, K.A., Cairns, P., Dravitzki, S., Bennie, S.L., Caldwell, T.G., Ogawa, Y., 2009. A magnetotelluric study of Mount Ruapehu volcano. *New Zealand. Geophysical Journal International*. doi:10.1111/j.1365-246X.2009.04317.x.
- Jolly, A.D., Sherburn, S., Jousset, P., Kilgour, G., 2010. Eruption source processes derived from seismic and acoustic observations of the 25 September 2007 Ruapehu eruption–North Island, New Zealand. *J. Volcanol. Geotherm. Res.* 191, 33–45.
- Kang, T.S., Shin, J.S., 2006. Surface-wave tomography from ambient seismic noise of accelerograph networks in southern Korea. *Geophys. Res. Lett.* 33, L17303.
- Kilgour, G., Jolly, A.D., Sherburn, S., Scott B.J., Miller, C. & Rae, A.J., 2007. The October, 2006 eruption of Ruapehu Crater Lake in *Mortimer, N., Wallace, L.* Joint GSNZ/NZGS conference, Tauranga, New Zealand. Programme & Abstracts.
- Kilgour, G., Manville, V., Della Pasqua, F., Graettinger, A., Hodgson, K.A., Jolly, G.E., 2010. The 25 September 2007 eruption of Mount Ruapehu, New Zealand: directed ballistics, surtseyan jets, and ice-slurry lahars. *J. Volcanol. Geotherm. Res.* 191, 1–14.
- Lin, F., Ritzwoller, M.H., Townend, J., Bannister, S., Savage, M., 2007. Ambient noise Rayleigh wave tomography of New Zealand. *Geophysical Journal International* 170, 649–666.
- Lu, Z., Masterlark, T., Power, J., Dzurisin, D., Wicks, C., 2002. Subsidence at Kiska volcano, Western Aleutians, detected by satellite radar interferometry. *Geophys. Res. Lett.* 29 (18), 1855.
- Manville, V., Cronin, S.J., 2007. Breakout lahar from New Zealand's crater lake. *Eos Trans. AGU* 88 (43).
- Manville, V., Graettinger, A., Hodgson, K.A., Mountain, B., Cronin, S.J., Lube, G., in preparation. Ice-slurry lahars triggered by the 25 September 2007 eruption of Mt. Ruapehu, New Zealand.
- Miller, V., Savage, M.K., 2001. Changes in seismic anisotropy after volcanic eruptions: evidence from Mount Ruapehu. *Science* 293, 2231–2233.
- Milbert, D., 2008. Solid Earth tides. <http://home.comcast.net/dmilbert/softs/solid.htm>.
- Mogi, K., 1958. Relations between the eruptions of various volcanoes and the deformations of the ground surfaces around them. *Bull. Earthquake Res. Inst.* 36, 99–134.
- Nakagawa, M., Wada, K., Thordarson, T., Wood, C.P., Gamble, J.A., 1999. Petrologic investigations of the 1995 and 1996 eruptions of Ruapehu volcano, New Zealand: formation of discrete and small magma pockets and their intermittent discharge. *Bull. Volcanol.* 61, 15–31.
- Niu, F., Silver, P.G., Daley, T.M., Cheng, X., Majer, E.L., 2008. Preseismic velocity changes observed from active source monitoring at the Parkfield SAFOD drill site. *Nature* 454, 204–208.
- Poupinet, G., Ellsworth, W.L., Frechet, J., 1984. Monitoring velocity variations in the crust using earthquake doublets: an application to the Calaveras fault, California. *Geophys. J. Res.* 89, 5719–5731.
- Ratdomopurbo, A., Poupinet, G., 1995. Monitoring a temporal change of seismic velocity in a volcano: application to the 1992 eruption of Mt. Merapi (Indonesia). *Geophys. Res. Lett.* 22 (7), 775–778.
- Rowlands, D.P., White, R.S., Haines, A.J., 2005. Seismic tomography of the Tongariro Volcanic Centre, New Zealand. *Geophys. J. Int.* 163, 1180–1194.
- Sens-Schönfelder, C., Wegler, U., 2006. Passive image interferometry and seasonal variations of seismic velocities at Merapi volcano, Indonesia. *Geophys. Res. Lett.* 33 L21302.
- Shapiro, N.M., Campillo, M., 2004. Emergence of broadband Rayleigh waves from correlations of the ambient seismic noise. *Geophys. Res. Lett.* 31 L07614.
- Shapiro, N.M., Campillo, M., Stehly, L., Ritzwoller, M.H., 2005. High-resolution surface wave tomography from ambient seismic noise. *Science* 307, 1615–1618.
- Sherburn, S., Bryan, C.J., Hurst, A.W., Latter, J.H., Scott, B.J., 1999. Seismicity of Ruapehu volcano, New Zealand, 1971–1996: a review. *J. Volcanol. Geotherm. Res.* 88, 255–278.
- Snieder, R., 2006. The theory of coda wave interferometry. *Pure Appl. Geophys.* 163, 455–473.
- Snieder, R., Grêt, A., Douma, H., Scales, J., 2002. Coda wave interferometry for estimating nonlinear behaviour in seismic velocity. *Science* 295, 2253–2255.
- Stehly, L., Campillo, M., Shapiro, N.M., 2006. A study of the seismic noise from its long range correlation properties. *J. Geophys. Res.* 111, B10306.
- Stehly, L., Fry, B., Campillo, M., Shapiro, N.M., Guibert, J., Baschi, L., Giardini, D., 2010. Tomography of the Alpine region from observations of seismic ambient noise. *J. Int.* 178, 338–350.
- Weaver, R.L., Lobkis, O.I., 2001. Ultrasonics without a Source: thermal fluctuation correlations at MHz frequencies. *Phys. Rev. Lett.* 87 (13), 134301.
- Wegler, U., Sens-Schönfelder, C., 2007. Fault zone monitoring with passive image interferometry. *Geophys. J. Int.* 168, 1029–1033.
- Wessel, P., Smith, W.H.F., 1998. New, improved version of the generic mapping tools released. *EOS Trans. AGU* 79.

**Fig. 17.** Deformation network and modelling. Top: Map of the GeoNet GPS and seismic network at Ruapehu (red dots and black squares respectively, with the blue lines representing the CCF lines). In grey are the locations of the two modelled Mogi sources (1 and 2). Bottom: results from the deformation modelling for the two sources. Crosses and circles respectively represent the modelled vertical ( $uz$ ) and horizontal ( $ux$  and  $uy$ ) displacements at the various GPS stations. The solid and dashed curves are the maximum vertical and horizontal displacement recordable over the whole network. The maximum radius for the two sources is given when these curves cross their corresponding instrumental detection limit.